



Computational analysis of the anterior cruciate ligament reconstruction under different graft configurations

C. Díaz-Cuadro¹ · H. Figueredo Losada¹ · D. Santos²

Received: 20 July 2021 / Accepted: 9 June 2022 / Published online: 25 June 2022
© Sociedade Brasileira de Engenharia Biomedica 2022

Abstract

Purpose The aim of this work is to computationally study the effect of anterior cruciate ligament reconstruction and to assess the sensitivity of joint biomechanics to changes in different parameters.

Methods This procedure consisted of three stages: firstly, the determination of the knee joint kinematics. This was inferred from motion capture of a patient repeating a motor task. The capture was made with a VICON system using skin markers on the patient; secondly, the setup of a finite element simulation of a healthy knee reproducing the same motor task, in the FEBio software; and finally the development of a model for a knee with single-bundle ACL reconstruction. Ten different settings of this model were analyzed.

Results The results show that a 10% variation in the mechanical properties of the ACL does not cause a significant change in the dynamic behavior of the healthy knee joint. No significant differences were observed in the ACLr with different materials, either. The location of the femoral tunnel that best restores the joint biomechanics is the one made in the center of the femoral footprint of the ACL.

Conclusion In general terms, the results of healthy KJ agree with those presented in the reference literature. Moreover, the forces and moments resulting from the reconstructions reaffirm that the optimal position for the location of the femoral insertion is the center of the original ACL footprint. In addition, it is concluded that the restoration of the biomechanics of the KJ is much more sensitive to the location of the femoral tunnel than to the mechanical properties of the graft, in the range of variations that were taken into account in this work.

Keywords Knee Joint · Motion Capture · FEM · ACL reconstruction

Introduction

The human body is a complex mechanical structure and the knee joint (KJ) and, particularly, is one of the most complex and demanded joint due to two facts: it has to carry very high loads and its structure must enable triaxial movements without losing both stability and motor control (Domenech et al. 2003; Góngora et al. 2003; Panesso et al. 2018; Trad et al. 2018). Besides, the anterior cruciate ligament (ACL) deficiency is one of the most common injuries of the KJ, affecting about one in 3000 people in the USA every year

(Kim et al. 2011; McLean et al. 2015; Mallett and Arruda 2017; Noyes et al. 1974), at the estimated cost of US\$ 10.000 per recovered patient (Santos 2014).

In spite of the scientific progress of the last fifty years, the long-term outcome of the ACL reconstruction (ACLR) shows a degradation of the articular kinematics, which could lead to early osteoarthritis (OA) (Tashman et al. 2021). Therefore, increasing the knowledge about the behavior of the KJ and the function and mechanical properties of each of its structures is necessary to improve treatments (Bae and Cho 2020; Marieswaran et al. 2018; Mallett and Arruda 2017; McLean et al. 2015; Siebold et al. 2014; Dienst et al. 2002; Jakob and Staübli 1992; Girgis et al. 1975; Noyes et al. 1974). Moreover, it is also necessary to develop new techniques that allow the evaluation of the outcome of the KJ with ACLR, in the least invasive way possible (Bistolfi et al. 2021; Guo et al. 2020; Barié et al. 2019; Todor et al. 2019; Kim et al. 2018).

✉ C. Díaz-Cuadro
cdiaz@fing.edu.uy

¹ Instituto de Ingeniería Mecánica Y Producción Industrial, Facultad de Ingeniería, UdelaR, Montevideo, Uruguay

² Departamento de Rehabilitación, Facultad de Medicina, UdelaR, Montevideo, Uruguay

In recent years, technological progress has exponentially increased the computing capacity of computers, allowing computational models to emerge as a good alternative to understand the mechanics involved in this complex joint. These models avoid both experimental difficulties and difficulties related to patients, financing or time availability (Pena et al. 2006; Trad et al. 2018; Rachmat 2015). Due to these facts, in the last forty years, mathematical models representing the knee joint's biomechanics and the interaction between its different structures have been frequently implemented.

To name but a few, Crowninshield et al. (1976) presented one of the first works that models the knee joint, evaluating the function of each of its main ligaments (represented by 13 structures) in the joint stability when it is subjected to external loads. Some years later, Wismans et al. (1980) present a work considering 3D geometries, in which bone surfaces are represented as rigid bodies and ligaments as nonlinear springs fixed to different points on the surfaces.

Later, Andriacchi et al. (1983), Essinger et al. (1989) y Blankevoort et al. (1991) developed mathematical models of the joint to study different effects. The first one models the knee's performance according to loads and restrictions. The second one studies the joint's biomechanics in terms of contact pressure and stress distribution for knees with condyle prostheses. The third one studies the characteristics of the articular contact with two different models.

In the late 1990s, 2D and 3D models analyzed by the finite element method (FEM) were developed. Their use in biomechanics has become a promising tool for the study and simulation of biosystems (Trad et al. 2018; Kazemi et al. 2013; Fregly et al. 2012; Ali et al. 2016; Cooper et al. 2019). The work presented by Li et al. (1999) was one of the first 3D analyses that study the tibia and femur joint through the FEM. This work predicted the joint kinematics and the forces on ligaments in response to external loads. The geometry in this work was obtained from an MRI of a cadaveric knee, and the cartilage was modeled as an elastic material, the menisci as groups of springs of equivalent stiffness, the ligaments as nonlinear springs and the bones as rigid bodies. The same specimen was tested in the universal force–moment sensor system, and the results presented a similarity that validated the computational model and boosted the development of more advanced models, showing the great potential of computational analysis on the effectiveness of ligament reconstruction. Since then, the KJ has been deeply studied in different aspects, such as the biomechanical response of each of its structures against external loads (Pena et al. 2006; Meng et al. 2014), the degeneration of articular cartilage (Halonen et al. 2014; Shirazi and Shirazi-Adl 2009), the influence of bone geometry and meniscal shape (Łuczkiwicz et al. 2015; Mootanah et al. 2014) and the biphasic response of cartilage (Meng et al.

2014; Räsänen et al. 2017; Meng et al. 2017), among many others. Nowadays, this method is the most popular and has been widely implemented in a large number of scientific publications (Trad et al. 2018; Kazemi et al. 2013; Fregly et al. 2012; Ali et al. 2016; Cooper et al. 2019) in the last 30 years to create 3D models of the KJ.

Many studies about the KJ have been carried out in both forms, *in vivo* and *in vitro*, and they showed a high variability of the mechanical properties from person to person and according to age (Tashman et al. 2021; Marra 2019; Naghibi Beidokhti 2018; Shu et al. 2018; Pena et al. 2006). Therefore, it is crucial to identify to what extent this variation can have an impact on the results of computational analyses.

The aim of this work is to take a first step toward the development of a procedure to computationally reproduce the specific knee joint of a patient, in order to be able to evaluate different scenarios in advance, in a totally noninvasive way. For example, to determine the optimal position for bone tunnels in an ACLr or to evaluate the evolution of the knee after an operation, given a high number of daily activities such as walking, sitting and standing or climbing a step, in order to prevent the appearance of joint degeneration.

In this work, subject-specific kinematic data were used as input for a 3D finite element model of the healthy KJ, both obtained in a noninvasive way. The main contribution of this work is the evaluation of the sensitivity of the results to variations in the mechanical properties of the material model. Moreover, a 3D finite element model of a KJ with ACLr was developed. The behavior of this model, as well as its alterations when varying the type of graft and the location of the femoral tunnel, was analyzed. It should be noted that in this work all the analyses are performed for the same kinematic condition, evaluating the dynamic response of the soft tissues, even in the case of the ACLr. In this way, the dynamic effect that the movement made by the patient has on the tissues, in different configurations but under the same boundary conditions, is compared.

Methods

As can be seen in Fig. 1, there are three well-differentiated stages that make up the work: the joint kinematics determination (stage 1), the setup of a finite element model of the healthy KJ (stage 2), and the development of a finite element model that simulates the ACLr (stage 3). Each stage can be separated into different stages as shown below.

Motion capture

To determine the joint kinematics, an experimental test that consists of capturing the movement of a patient using stereophotogrammetry was carried out. As the aim of this work is

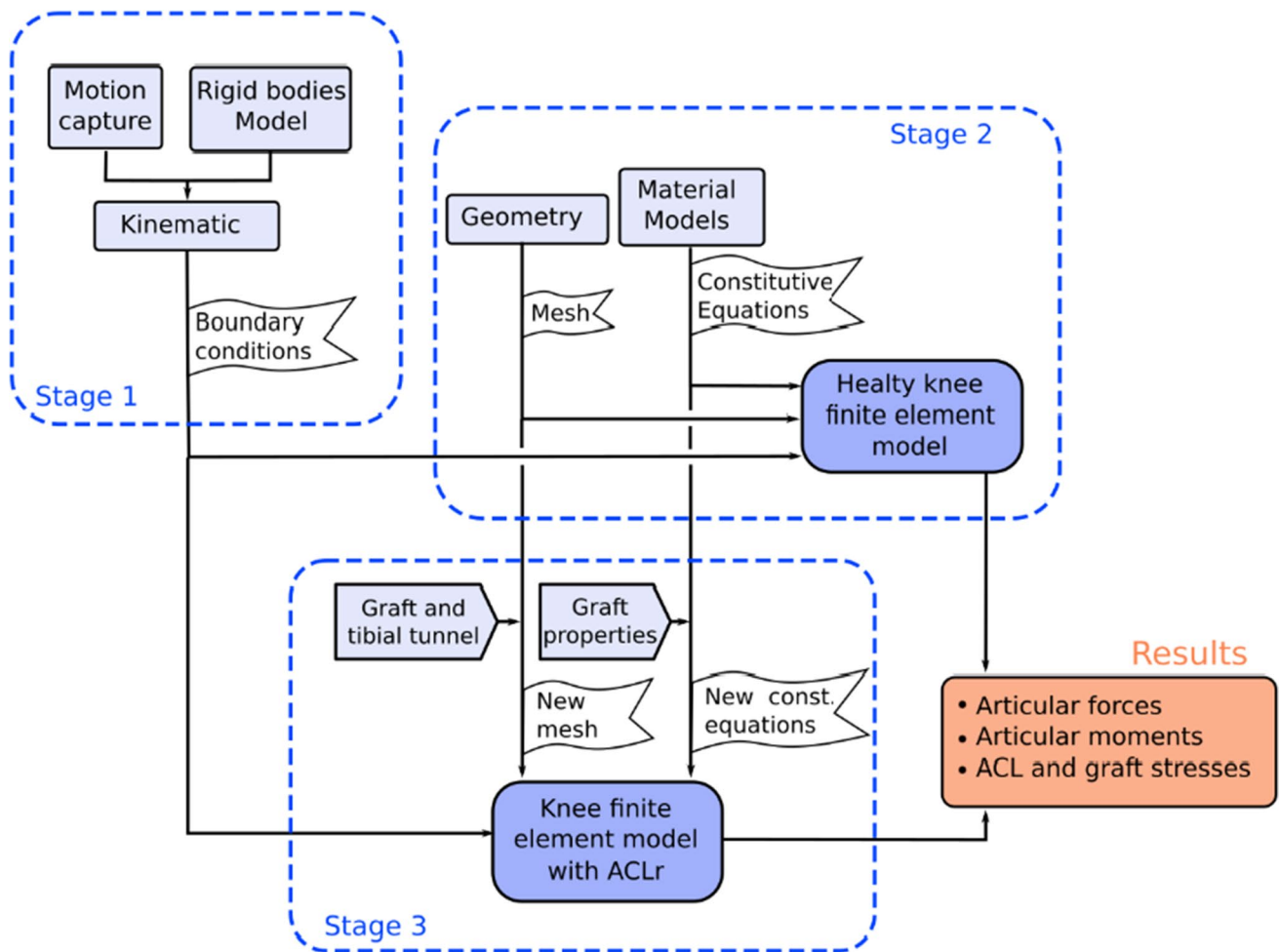


Fig. 1 Flowchart of the developed procedure

to show the feasibility of developing a patient-specific knee model with specific motion data of that patient, we only captured his kinematics.

For the motion capture, a healthy 50-year-old man, without knee joint pathologies that affect the normal development of the chosen motor task, was selected. This study was carried out in the gait laboratory of the Hospital de Clínicas, which has a VICON system with 8 infrared cameras that cover a volume of approximately 5mx7mx2,5m.

Before starting the experiment, the necessary anthropometric measurements of the patient were taken: height 172 cm, distance between iliac spines 28 cm, limb length 88 cm (right) 87,5 cm (left), right knee width 90 mm, and right ankle width 70 mm.

The reflective markers were placed on the patient’s skin following the protocol established by the modified plug-in gait model (mPiG) (Kadaba et al. 1990; VICON 2017), as can be seen in Fig. 2. Static calibration, which consists of filming the patient with the 20 markers for one second while he is motionless, was performed (see Fig. 2a).

The mPiG model consists in seven structures, which represent the pelvis, femur (x2), tibia (x2), and foot (x2), and six spherical joints that allow three degrees of freedom (DoF), which play the role of real joints. Although real human joints are much more complex than spherical joints because they have 6 DoF instead of 3, the translation DoF is neglected with this model, because these particular movements have the same order as the error on motion capture technique.

Once the static calibration was finished, the volunteer was asked to repeat the task of climbing the step in Fig. 2b ten times as similarly as possible, while he was being recorded with the Vicon system.

The data obtained from this experiment are shown in Fig. 3, where the value of the angles of flexo-extension (FE), internal–external rotation (IE), and varum–valgum rotation (VV) can be seen.

Figure 3 shows a high range of varum–valgum motion in contrast to what can be found in the literature. In fact, the common range for this parameter is $12^\circ \pm 2^\circ$ (Chhabra



Fig. 2 **a** Markers location over the patient. **b** Patient climbing the step

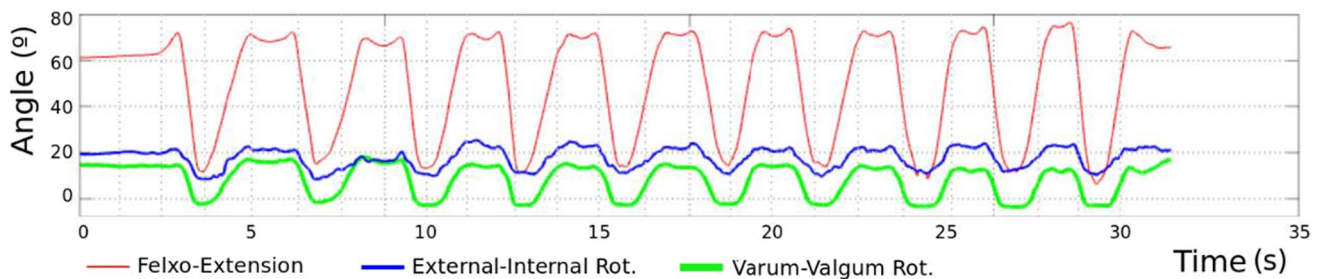


Fig. 3 Angles of the knee joint

et al. 2001; Jakob and Stäubli 1992). This indicates a clear overestimation of the VV angle that can be attributed to cross talk or soft tissue artifact (Andersen et al. 2010; Charlton et al. 2004; Chiari et al. 2005; Leardini et al. 2005; Stief et al. 2013). For this reason, this curve was not used for the boundary condition.

Knee joint model

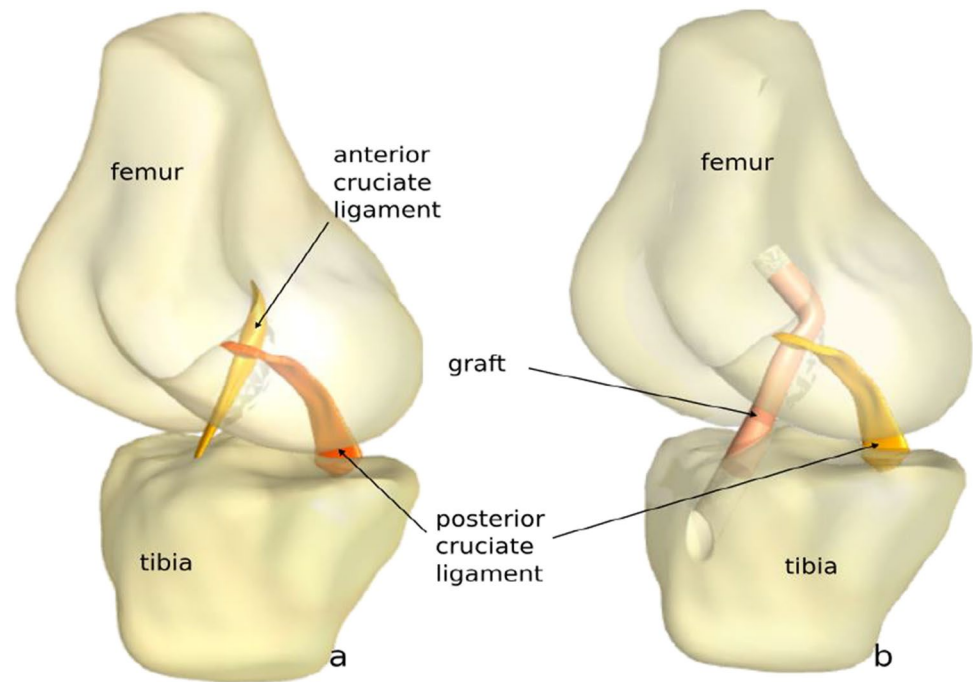
Any 3D finite element model consists of three parts: firstly, the determination of the geometry of each structure that was taken into account in the simulation; secondly, the description of the mechanical behavior of each of these structures; and finally, the discretization of the domain, the

application of the boundary conditions and the constraints and setting of the simulation parameters.

Geometry of the joint

This work used the geometry shared by the open knees project (Erdemir 2013; Sibole et al. 2010), which provides open access to 3D finite element representation of the knee joint for research, development, and experimentation to enlarge the knowledge on this topic. Although the original geometry has eleven different structures, for this work, only those that directly interact with the ACL were taken into account. This aspect leads to a simplification of the eleven-structure system to a four-structure system, containing femur, tibia, posterior cruciate ligament (PCL), and ACL or graft (see Fig. 4).

Fig. 4 **a** Four structures of the healthy KJ. **b** Four structures of the KJ with ACLr



Geometry of bone tunnels

Although there are several techniques to perform this reconstruction, the trend nowadays, which we followed in this work, is to perform the technique with an anteromedial portal (Tashman et al. 2021; Rothrauff et al. 2020; Kim et al. 2018). In this technique, both bone tunnels are made independently: while the tibial tunnel is made in the classical way, the femoral tunnel is made from an open portal in the anteromedial (AM) zone of the KJ. This is done in order to reach in both cases, the bony insertions of the original ligament (Bedi et al. 2011; Bonnin et al. 2012). In this work, the “anterior cruciate ligament reconstruction: a practical surgical guide” (Siebold et al. 2014), which shows the procedure to perform the tunnels, is followed.

The tibial tunnel is fully determined by the definition of two angles (sagittal and coronal) and the location of the tibial footprint of the ACL. According to the guide (Siebold et al. 2014), the suggested sagittal angle should be kept between 40 and 50°, while the coronal angle should be 25° (Fig 5a).

The femoral tunnel is performed through an anteromedial portal, while the tibia is totally vertical and the flexion angle is beyond 120° (Fig 5b). The tunnel is drilled in this position, pointing to the femoral footprint of the ACL, with a horizontal orientation, and with the largest transverse angle possible (Fig 5b) (Siebold et al. 2014).

In addition, we studied the effect of moving the insertion site of the femoral tunnel 3mm in three different directions, proximal (P), distal (D), and anterior (A), from the center of

the ACL footprint (o) (Fig 6), and the results in each direction were compared to the results in the other two.

Geometry of graft

Since the objective of the work is to study the effect of the inserts and their mechanical properties, all the grafts were created in the same way, have the same geometry and were studied under the same kinematics. The Siebold et al. (2014) guide shows a table for selecting the diameter of the tunnel to be made, based on the sagittal angle of incidence in the tibia and the dimensions of the original insertion of the ligament, if any. In this case, with an angle of 55° and the measurement of the femoral insertion, a drilling diameter $d = 6.5$ mm is suggested (cross-sectional area = 33mm²). On this basis the graft is created so that the ends match the size of the tunnel. Guide ellipses are created along the way (see Fig. 7), acting as guides to maintain a similar shape with each other and avoiding crossing the posterior cruciate ligament.

Materials

Bones: These structures were modeled as rigid bodies, since their deformation is negligible compared to that of the ligaments.

Ligaments: As a soft tissue, ligaments present high strains; therefore, it is necessary to use a stress–strain relationship that allows its modeling. In the case of ligaments and tendons, there is a consensus to model them as transversely isotropic hyperplastic (TIH) structures because of their nature

Fig. 5 **a** Location of the tibial tunnel. **b** Location of the femoral tunnel

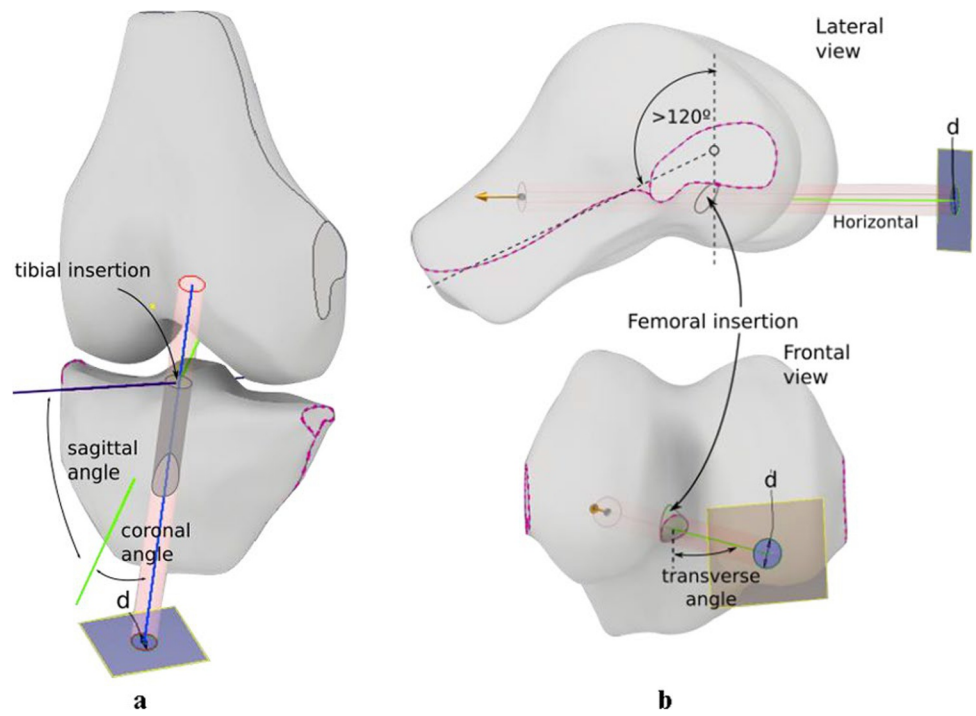


Fig. 6 Variations in the insertion of the femoral tunnel

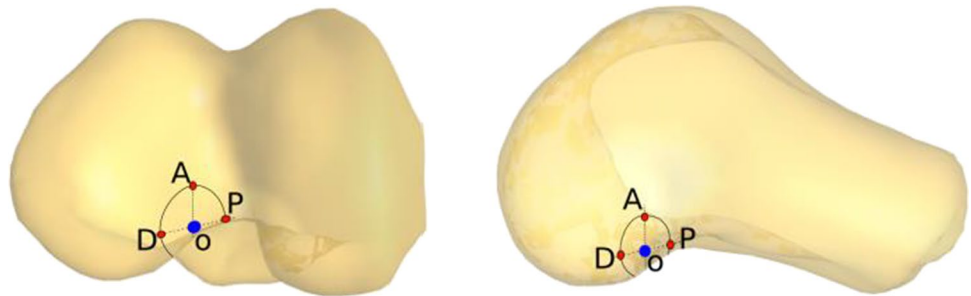
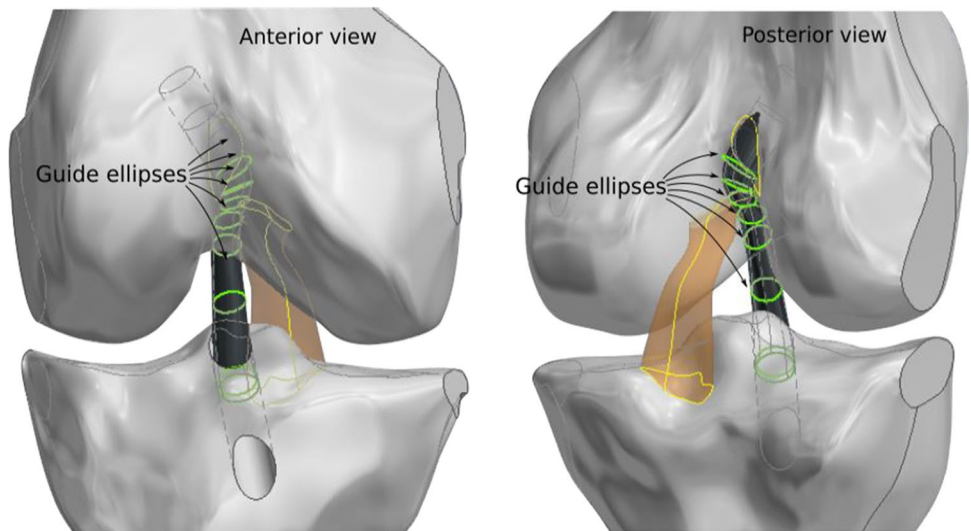


Fig. 7 Ellipses that guide the graft



of fibril-reinforced materials. Their main direction, in which they are stiffer than in the others, is the longitudinal direction. Weiss et al. (1996) developed the strain energy density (Ψ) for this type of material, starting by separating the matrix substance's (m) energy from the fibers' energy (f), as it is shown in Eq. 1.

$$\Psi(C, a^\circ) = \Psi^m(C) + \Psi^f(C, a^\circ) \tag{1}$$

where C is the right Cauchy strain tensor, and $a0$ is the orientation of the fibers in reference configuration. Assuming that the behavior of the matrix substance can be modeled as Mooney–Rivlin material, we have Eq. 2, in which C_1 and C_2 are material's constants, K is the bulk modulus and I_i is the i^{th} invariant of C :

$$\Psi^m(C) = C_1(\tilde{I}_1 - 3) + C_2(\tilde{I}_2 - 3) + \frac{K}{2} \ln\left(\sqrt{\tilde{I}_3}\right)^2 \tag{2}$$

In Eq. 2, the strain energy density function of the matrix substance is separated into its deviatoric and volumetric components (Weiss 1994; Weiss et al. 1996), where the first two terms correspond to the deviatoric part of the deformation (using the $\tilde{\cdot}$ symbol for identification). The third term in Eq. 2 is a penalty function of the volume change of the body.

Weiss (1994) proposed the functional form of the term ψ^f of Eq. 1, as a function of the fibers' stretching $\lambda = L/L_0$, as seen in Eq. 3.

$$\lambda \frac{\partial \Psi^f}{\partial \lambda} = \left\{ \begin{array}{ll} 0 & \lambda < 1 \\ C_3 (e^{C_4(\lambda-1)} - 1) & 1 < \lambda < \lambda^* \\ C_5\lambda + C_6 & \lambda > \lambda^* \end{array} \right\} \tag{3}$$

where C_3 , C_4 , and C_5 are material's constants and λ^* is the stretch in which all the fibers are recruited and start the linear behavior.

As can be seen in Eqs. 2 and 3, this material's modeling needs seven parameters. The ones used for the ACL and the PCL were the same as in Pena et al. (2006), which were inferred from (Łuczkiwicz et al. 2015; Weiss et al. 2002) (see Table 1).

Moreover, four more models of the ACL were created to analyze the absence of fibers (N–H model) and variability in 10% less of the material's constants (90% models). The new model parameters are summarized in Table 2.

Grafts: Three of the most used grafts were analyzed: patellar tendon (PT), semitendinosus (ST), and gracilis (Gr). The constitutive relationship used is the same as for the original ligament (TIH) since the grafts are taken from similar structures. For the mechanical properties, those presented in the work of Pena et al. (2005) were used. These were inferred from adjusting the curves of the study of Suggs et al. (2003), which computationally models an ACLr with the same graft types as in the present work. The properties used, which define the transversely isotropic model, are shown in Table 3.

Mesh and Simulation settings

The discretization of the geometry was done with the 3D mesh generator Gmsh (Geuzaine and Remacle, 2009), which allows to select both the element size and where to refine the mesh. After a mesh convergence analysis, an acceptable precision of the results was reached using the number

Table 1 Properties of the LCA and the PCL for the TIH model extracted from (Pena et al. 2006)

	C1(MPa)	K(MPa)	C2(MPa)	C3(MPa)	C4	C5(MPa)	λ^*
ACL	1.95	73.21	0	0.0139	116.22	535.039	1.046
PCL	3.25	121.95	0	0.1196	87.178	431.036	1.035

Table 2 Variation of the properties of the LCA for the TIH model

Model	C1(MPa)	K(MPa)	C2(MPa)	C3(MPa)	C4	C5(MPa)	λ^*
N–H	1.95	73.21	0	0.0000	0.00	0.000	0.000
90%C1	1.75	73.21	0	0.0139	116.22	535.039	1.046
90%K	1.95	65.89	0	0.0139	116.22	535.039	1.046
90%C5	1.95	73.21	0	0.0139	116.22	481.535	1.035

Table 3 Properties used for PT, ST, and Gr graft model (Pena et al. 2005)

Graft type	C1(MPa)	K(MPa)	C2(MPa)	C3(MPa)	C4	C5(MPa)	λ^*
PT	2.75	206.6	0	0.065	115.89	777.56	1.042
ST	2.75	206.6	0	0.065	115.89	512.73	1.042
Gr	2.75	206.6	0	0.065	115.89	791.40	1.042

of elements for each structure shown in Table 4. Obtained computing times were reasonable for these configurations.

The computation of all the proposed finite element problems was solved by using the FEBio software (Maas et al. 2012), which is a nonlinear finite element solver that is specifically designed for biomechanics and biophysics applications. The resolution of the problem was found quasi-statically, with an adaptive time step according to the tolerance requested in the displacement (0.1%) and in the deformation energy (1%). The Broyden–Fletcher–Goldfarb–Shanno (BFGS) algorithm, which does not need to make a matrix inversion, was used.

In summary, five cases of the healthy knee model were simulated to analyze the sensitivity of the results: the original, the N–H, the 90%K, the 90%C1, and the 90%C5. Additionally, for the ACLr model, six simulations were performed. Three of them correspond to the three variations of the femoral insertion, which are performed with the same graft model (PT) to facilitate comparison. The other three correspond to each of the different types of grafts that were used (inserted in the original position). These simulations will be referred to hereinafter as follows:

- oPTr: Original patellar tendon reconstruction.
- aPTr: Anterior patellar tendon reconstruction.
- pPTr: Proximal patellar tendon reconstruction.

Table 4 Mesh parameters of each structure

Structure	Form	Nodes	Quantity	Avg. volume (mm ³)
Femur	tetrahedra	4	15,759	8.6
Tibia	tetrahedra	4	9297	8.2
ACL	tetrahedra	10	146,442	0.003
PCL	tetrahedra	4	28,159	0.025
Drilled femur	tetrahedra	4	31,630	4.269
Drilled tibia	tetrahedra	4	28,158	2.688
Graft	tetrahedra	10	~128,600	~0.009

- dPTr: Distal patellar tendon reconstruction.
- oSTr: Original semitendinosus reconstruction.
- oGrr: Original gracilis reconstruction.

Results

This section is divided into two parts, the first one showing the results for the five cases of the healthy knee joint model, and the second one presenting the results for the six cases of the knee joint with the ACLr.

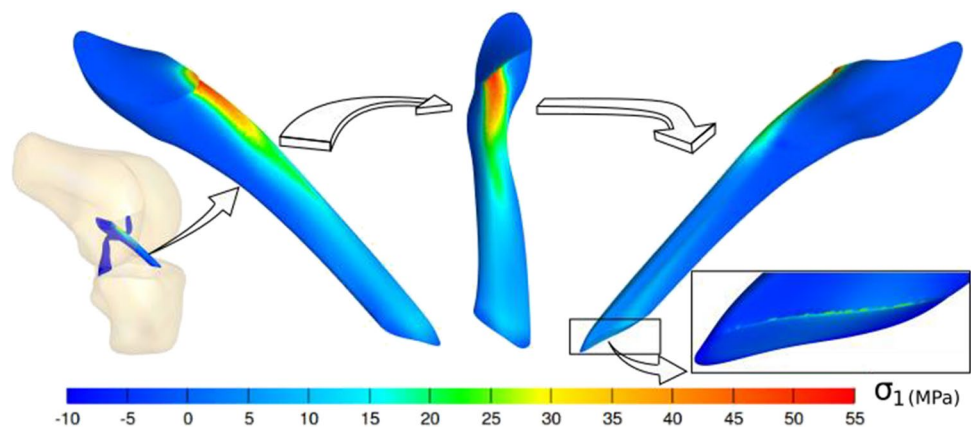
Healthy Knee models

Figure 8 shows the principal stress distribution for the ACL with the TIH model at the moment of highest loads, which was found at 55° of flexion.

Figure 8 shows, at the left, the position of the KJ at 55° of flexion. Then, a zoom of the ACL at that moment shows that the most critical zone is the anterior part, near to the femoral attach, which agreed with the literature (Bonnin et al. 2012; Butler et al. 1992; McLean et al. 2015). Furthermore, the maximum principal stress reached is 52 MPa, which also agrees with the range presented in Pena et al. (2006) and Fernandes (2014), in which similar situations are tested. In addition, on the right side of Fig. 8, a detailed capture of the posterior zone of the tibial ACL attach is shown. Some relatively high stress values are observed at the edge. This could occur because that zone has geometrical and material discontinuities, and also because in some cases, the fibril-reinforced model can have issues in this kind of region.

Figure 9 shows a comparison of the forces and torques caused by ligaments on the femur, while varying the mechanical properties of the ligaments. Considering the fact that during flexion the PCL is slack, the forces that it can perform are negligible compared to those of the ACL, which is tightened. Therefore, all the loads that can be seen in Fig. 9 are developed almost entirely by the ACL.

Fig. 8 First principal stress distribution on the ACL modeled as TIH



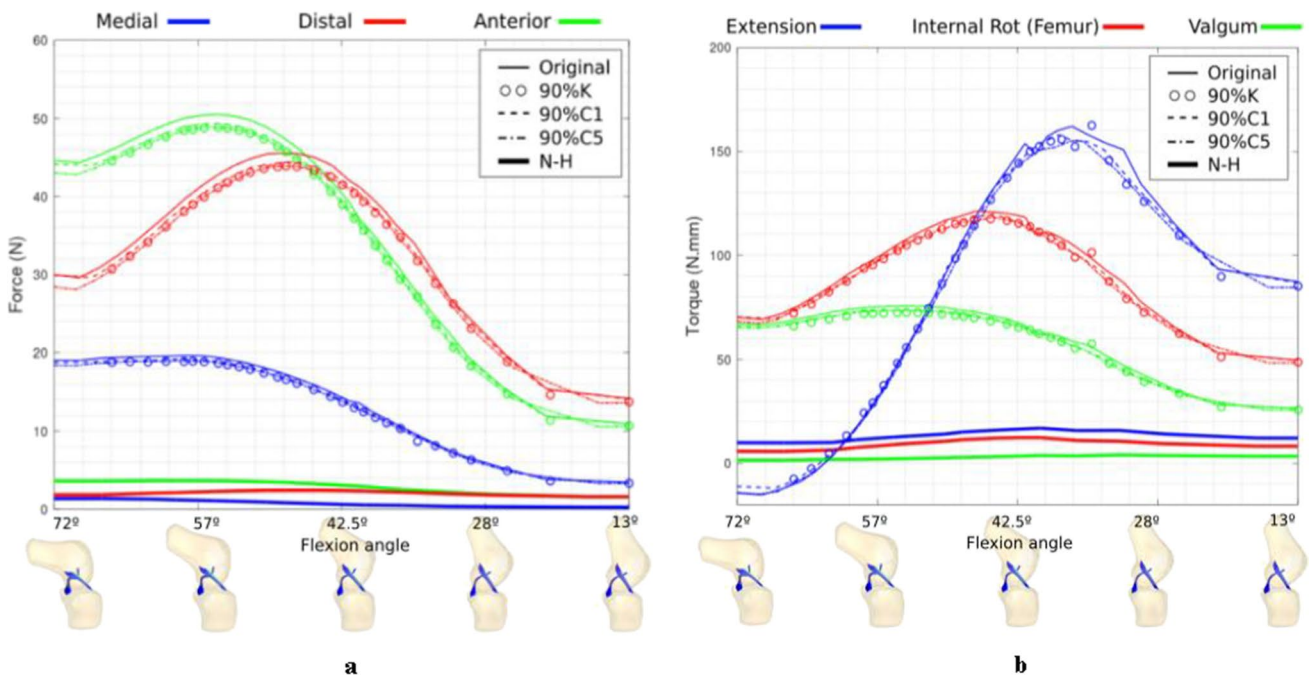


Fig. 9 **a** Comparison of forces on the femur in anatomical directions when the properties vary. **b** Comparison of torques on the femur in anatomical directions when the properties vary

Figure 9a shows that the femur is mainly forced distally and anteriorly, which matches with the direction of the ACL and is also consistent with the function of the ACL of avoiding the femoral posterior translation (tibial anterior translation) as was expected. The femur is also forced in the medial direction but with a lower magnitude.

On the other hand, Fig. 9b shows that the highest torques correspond to the restriction against the flexion of the KJ. The torques corresponding to the restriction against the external rotation of the femur are of a lower magnitude, and finally, the torques that avoid the varum rotation are the lowest in magnitude. These results are consistent with the respective importance of the different functions to be performed by the ACL (Siebold et al. 2014). Both Fig. 9a and 9b show that the differences between the models with a reduction of 10% in some properties (90% models) and the original model are negligible, since the highest variations are 1 N in forces and less than 10 Nmm in torques. However, the effect of not taking into account the fibers has a great impact in the results, decreasing close to 90% the restrictions over the joint.

ACLr models with different materials

Figure 10 shows the von Mises equivalent stress distribution at the instant where the maximum for each of the types of grafts studied was found. As in ACL, the most loaded area of the graft is near the femoral insertion on the anterior side, although in these cases it is a more localized

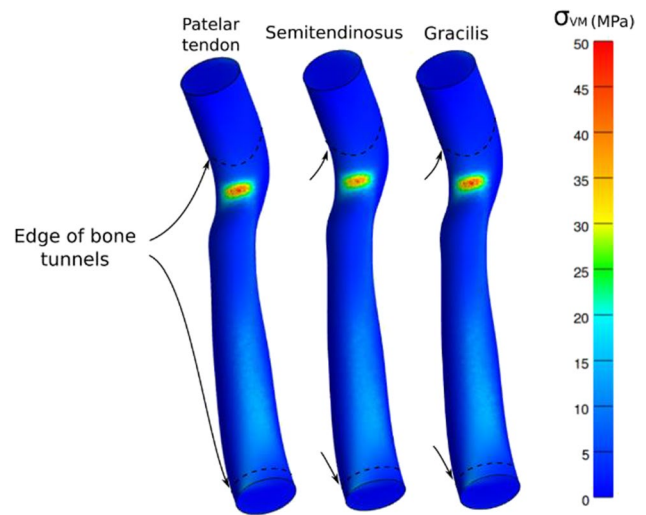


Fig. 10 Von Mises equivalent stress distribution for the three different grafts

region. The maximum equivalent stress for the three cases is around 50 MPa, indicating that the first principal stress is even lower than that of the ACL (see Fig. 8). In addition, Fig. 10 shows that the differences between the three grafts are imperceptible.

The graphs that show the comparison between the forces and the torques that the new grafts cause on the femur are shown in Fig. 11a and 11b. In both, it is

appreciated that the loads generated by the grafts present a similar trend to that of the model with the ACL. However, in Fig. 11a the forces of the graft are 40 to 50% lower than those of the ACL, and in Fig. 11b, the torques are 20 to 40% lower than those caused by the ACL.

ACLr models with different femoral insertions

Figure 12 shows the distribution of von Mises equivalent stress for models dPTr, aPTr, and pPTr, from left to right,

respectively, with two captures each, corresponding to the maximum flexion (72°) and maximum extension (13°) registered in this motor task.

It can also be seen in Fig. 12 that the three new insertions caused different inclinations from the ACL that has an angle of approximately 8° from the vertical. The proximal insertion shows a more vertical graft (6°), while the rest of them has a more oblique orientation (15° and 12°). Furthermore, the von Mises equivalent stress distribution is considerably higher for the anterior reconstruction (aPTr) with a maximum of 80 MPa.

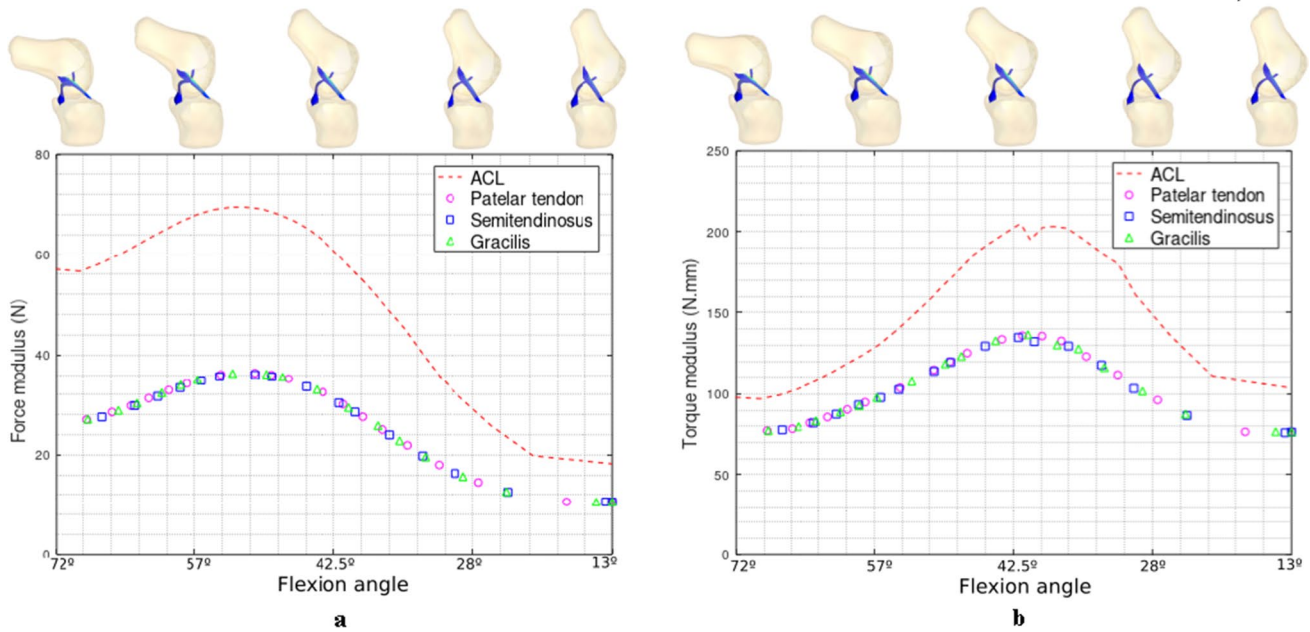


Fig. 11 a Comparison of forces on the femur. b Comparison of torques on the femur

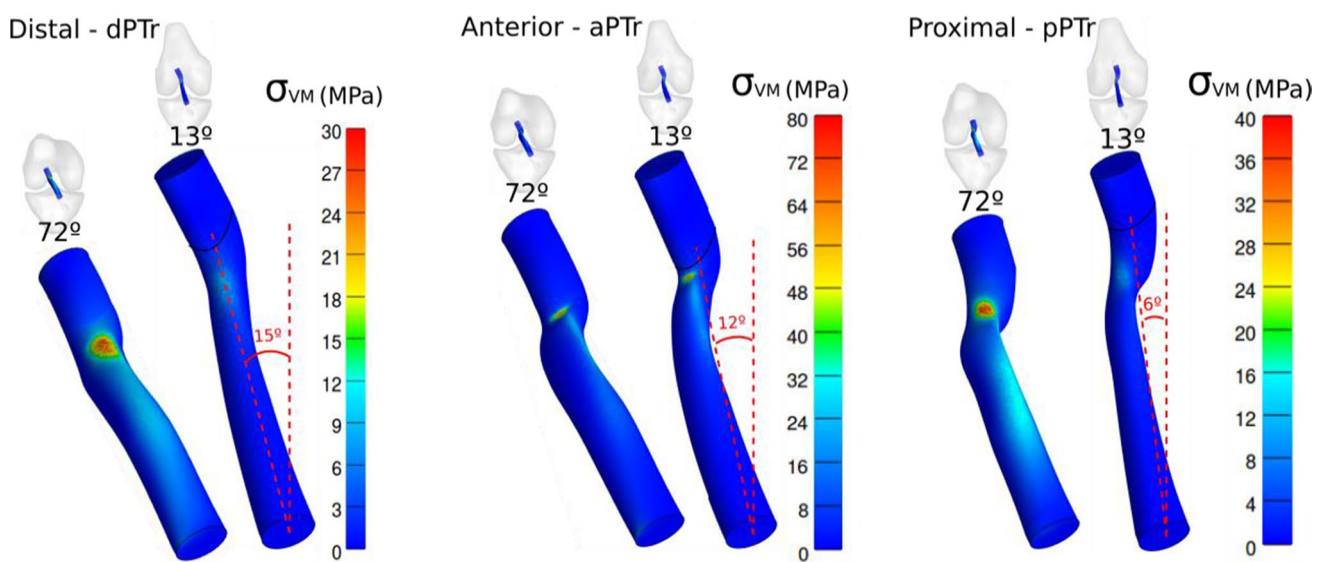


Fig. 12 Von Mises equivalent stress distribution and initial angles in the grafts with different femoral insertions

For the other two cases (pPTr, dPTr), the maximum (30 and 40 MPa) are slightly lower to that of the ACL (50 MPa). The three grafts show that their highest values of stress are in the same zone as in the ACL (anterior and proximal); however, while the dPTr and pPTr models show an area of similar size, the highest stresses in the aPTr model are more localized.

Next, the effect that the variations of the femoral tunnel have on the loads on the femur, for the same boundary conditions, is analyzed. Three graphs are presented (Fig. 13) showing the comparison between the forces generated by the model with the ACL and the reconstructions in each of the four perforations, and other three (Fig. 14), presenting the comparison between torques.

As previously shown (Fig. 11), the ACL and the reconstruction at the origin show, in general terms, the same trends. In terms of forces (Fig. 13), the grafts out of the origin also show a similar behavior for positions close to full extension. However, in deep flexion (beyond 45°) they exhibit a difference of up to 30% in terms of forces, compared to the oPTr model. It is worth noting that in no case does the change in femoral insertion cause the forces necessary to equalize the kinetic restraint imposed by the ACL.

In regard to the torques on the femur, the differences and the variability of the results are considerably higher than that of the forces. In the three figures (Fig. 14), it can be seen that the restrictions are again less than those generated by the ACL and even less (in most cases) than those caused by the oPTr model. In addition, the pPTr is the most inefficient reconstruction, showing the least constraint of the three models. In particular, in Fig. 14b the torques are about 15% of those caused by the ACL.

On the other hand, the aPTr and dPTr have a better behavior than the pPTr. However, in the case of the extensor torque and the torque toward varus (Fig. 14a and 14b, respectively), they show a lack of constraint in flexion angles beyond 45°, as compared to that of the reconstruction at the origin. In Fig. 14b, only the dPTr presents better results (closer to that of the ACL) and just for flexion angles less than 45°. With respect to the internal rotation torque (Fig. 14c), the aPTr and dPTr models improve the results obtained by the oPTr, getting closer to the loads of the ACL from 40° to full flexion.

Discussion

Limitations

This work, as all works, has its limitations. The geometry used does not correspond to the patient from whom the joint kinematics were taken, so the model is not strictly patient-specific. However, since the same geometry and the same kinematic conditions were used in all the models, the results can be compared.

This work used the 3D geometry and the kinematics of one single patient, so the numerical results obtained are not representative of the entire possible universe of patients. However, the qualitative results and the comparisons among them are still valid as they are evaluated under equal conditions.

The ligaments were considered as transversely isotropic hyperelastic materials because it is the model that is best adapted to their biomechanical behavior [Bae and Cho 2020; Naghibi Beidokhti 2018; Trade et al. 2018; Kim et al. 2018; Marieswaran et al. 2018; Halonen et al. 2016; Fernandez 2014; Pena et al. 2006; Pena et al. 2005; Weiss et al. 2002]; however, different properties were not considered for each of the two bundles of each ligament.

Possibly the most important limitation of this work is the simplification of modeling the 6-DoF knee joint with 3 DoF, together with the elimination of the data corresponding to VV rotation. To obtain a more precise FE model, a kinematic model that allows the kinematic results to be extracted at the corresponding 6 degrees of freedom must be made.

For ACLr analysis, no pre-tension was placed on the graft. This implies that the results could vary if any value is considered. However, since it is not a standardized procedure in practice, it was decided to make the comparison without pre-tension in the ACLr procedure.

Healthy Knee

The results of the healthy KJ, using a transversely isotropic hyperelastic material to model the ligaments, show that in the movement of climbing a step, the most loaded zone of the ACL is its anterior and proximal part (Fig 8), which agreed with the literature (Xiao et al. 2021; McLean et al. 2015; Bonnin et al. 2012; Butler et al. 1992). A further analysis shows that variation in 10% in mechanical properties of the models does not cause any significant effect in the joint mechanics (Fig 9), since the changes are less than 2N in forces and 10 Nmm in torques. However, if fibers are not taken into account, it is necessary to use an equivalent Young's modulus, instead of the real properties of the matrix substance, to obtain a more representative result.

In terms of forces, the results show that they increase with the flexion angle up to a certain point between 45° and 55°, depending on the direction (Fig 9a). The maximum forces reached are 50N, 45N and 18N for the anterior, distal, and medial force, respectively. From the maximum point, all forces decrease with the flexion angle, except for the medial force, which stays close to the 18N. Compared to the theoretical results presented by Shelburne et al. (2004) and with the cadaveric studies carried out by Markolf et al. (1995), the forces obtained here are considerably lower. This can be directly associated with the fact that the input variable of the models (kinematics) was obtained from an indirect method

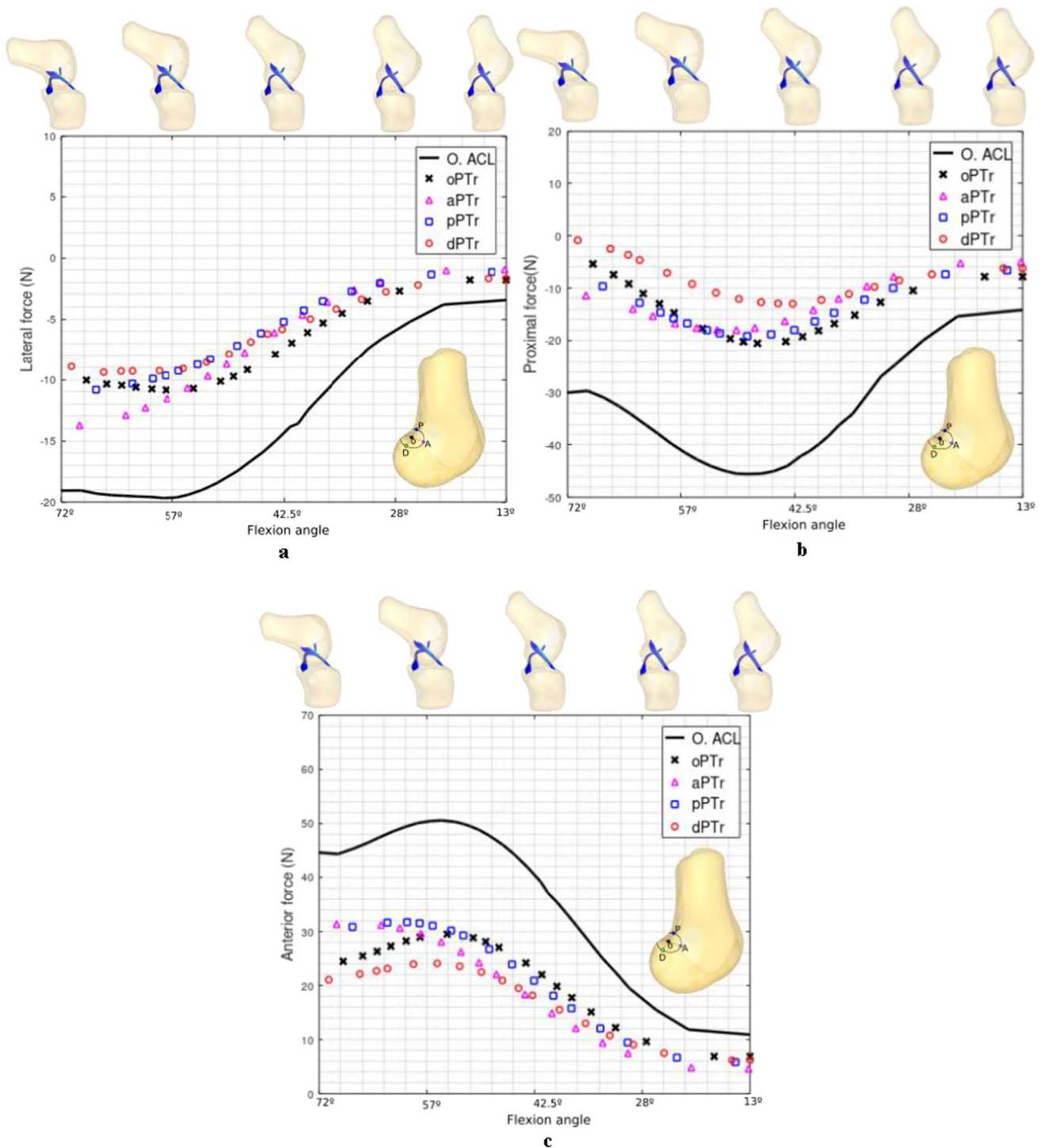


Fig. 13 **a** Comparison of forces in lateral direction on the femur. **b** Comparison of forces in proximal direction on the femur. **c** Comparison of forces in anterior direction on the femur

(motion capture), which admits errors of millimeters (Chiari et al. 2005; Leardini et al. 2005), which translate into high loads. Differences in forces are also transmitted to torques; therefore, it is useless to analyze these results quantitatively.

However, the qualitative analysis of the ligament behavior is of interest, since it shows that its main functions are to avoid posterior translation of femur (Fig. 9a) and to provide stability during flexion and internal–external rotation (Fig. 9b).

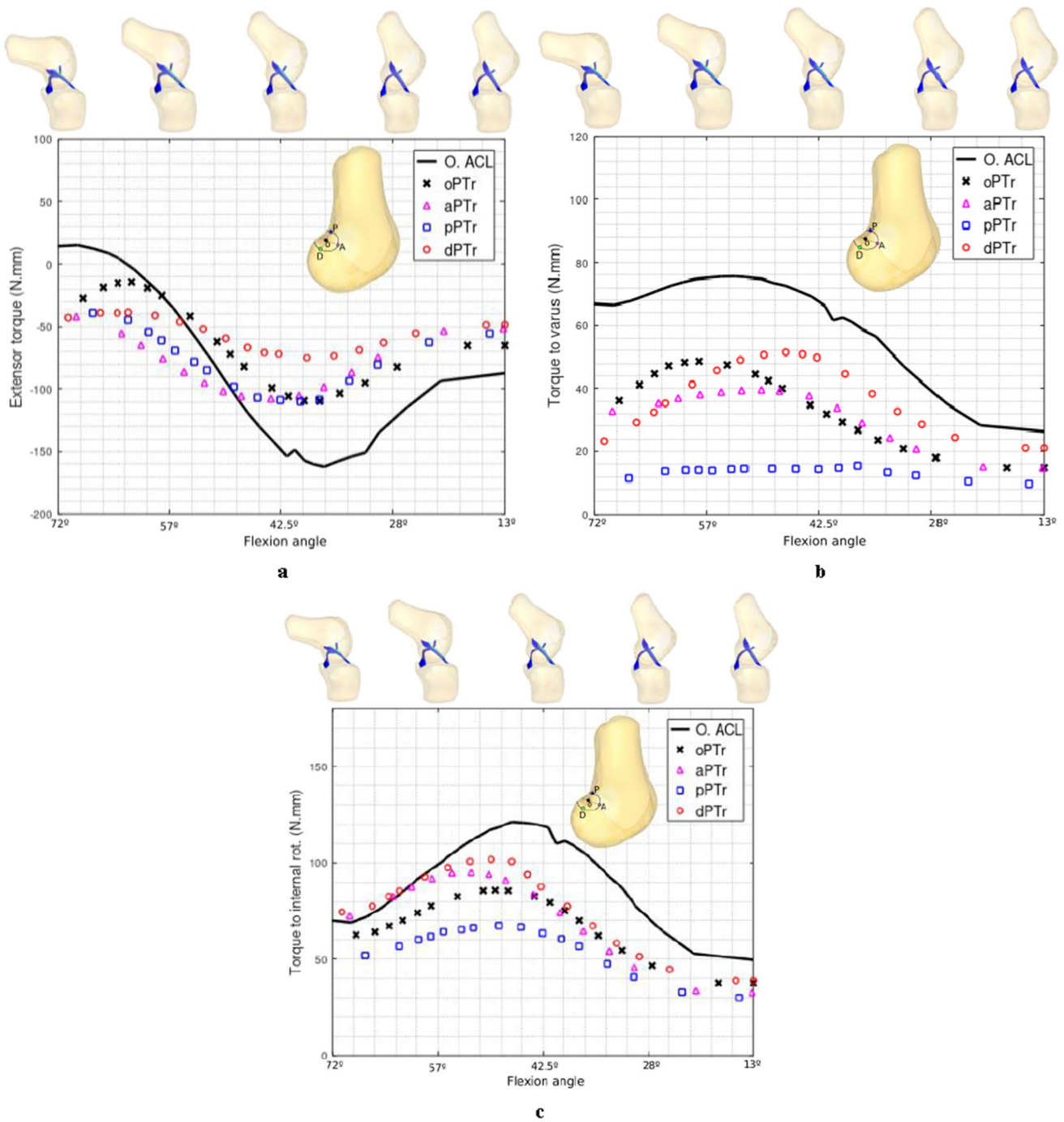


Fig. 14 **a** Comparison of extensor torques on the femur. **b** Comparison of torques to varus on the femur. **c** Comparison of torques to internal rotation on the femur

ACLR with different materials

The differences between the stress distribution (Fig. 10) and the behavior (Fig. 11) of the three grafts are practically imperceptible. This indicates that if the material models and the properties used are sufficiently correct, the distribution of the stresses does not appear to change with variation in properties

for the values selected. This finding agrees with the results of Chen et al. (2019), who did not find any significant difference between patellar tendon and hamstring behavior. In addition, Todor et al. (2019) and Barié et al. (2019) presented results of the comparative behavior of hamstring and quadriceps tendon as graft, and they did not find any significant difference neither in terms of stability, nor in outcomes for patients.

There is a clear difference between the loads exerted by the ACL and the grafts (Fig. 11) for both, forces and torques. Considering the mechanical properties are correct, these results indicate that the cross-sectional area of the graft should be greater. In the study by Miller and Gladstone (2002), all the proposed areas are greater than 35 mm², while in the present work the cross-sectional area of the graft used was 33mm². Thus, these results show that the procedure suggested by the guide (Siebold et al. 2014) overestimated the stiffness of the graft.

ACLR with different femoral insertions

With respect to the placement of the femoral insertion, the four models have a different performance in regard to stress distribution, forces, and torques. As expected, different insertions cause different inclinations on the graft (Fig 12), and this implies great variabilities mainly in torque on the femur (Fig 14). The results of the forces shown in Fig. 13 evidence greater differences as the flexion angle increases. The same effect appears in the work of Xiao et al. (2021), in which by means of the finite element method, different scenarios for different femoral tunnels are evaluated. In Figure 14a, it can be seen that the distal reconstruction model (dPTr) does not fulfill its function, while in Fig. 14a, the posterior reconstruction model (pPTr) is the one that is completely inefficient. The dPTr and aPTr should not be taken as successful, since in Fig. 14c both curves increase even beyond the curve corresponding to the ACL. That means that if the cross-sectional area is increased to the correct value, the curve of dPTr and aPTr will increase, over-constraining the joint. The only model that has a promising performance for all cases, taking into account the smaller area, is the oPTr.

Conclusion

We developed a procedure that allows the use of experimental data of motion capture on a FE generic model, with the aim of using subject-specific material properties and geometry in the near future. This work also shows that the results obtained with these steps reach similar qualitative results than other works (Bonnin et al. 2012; Butler et al. 1992; Fernandes 2014; McLean et al. 2015; Pena et al. 2006, 2005), which indicates that this could be a novel way to assess the state of the KJ health. However, in order to be able to obtain more reliable results to do a quantitative analysis, the input data should be improved. These improvements could be done by coming up with a way to deal with soft tissue artifact (Chiari et al. 2005; Leardini et al. 2005) or by using a different way of acquiring data.

The results of the healthy KJ confirm that in a daily movement such as climbing a step, the ACL plays a key role in providing stability to the KJ. In addition, it was shown that the loads performed by the ACL on the femur (mainly anterior and distal force, and moments that avoid the varus and external rotation) agree with the main functions of the ACL, which, in general terms, is to allow controlled movements. Furthermore, all the loads caused by the ACL present a maximum value around the 55° of flexion, which means that, for this case, the most critical stress distribution is found in that position.

In terms of material properties, we found that for a variability of 10% in their values, they do not significantly affect the kinematics. However, it turns out that it is important to take into account the fibers stiffness when fibrous materials are modeled, since the contribution of the ground substance to the ACL stiffness is approximately 10% of the total stiffness.

As for ACLr with different material properties, the results obtained, with the properties proposed in the work of Pena et al. (2005), are interesting, since they indicate that the results for both the stress distribution (and deformations) and the joint dynamics are indifferent when choosing a semiten-dinosus, patellar tendon or gracilis graft. It should be noted that the properties used were for a generic case; however, it is widely recognized the high variability of human soft tissue material properties. Therefore, it is concluded that for changes in the material properties as those presented in this work, the effects on the joint are not appreciable. Therefore, other factors must be considered for the selection of the type of graft to be used, among others: surgeon's expertise with each technique, effects of extraction, weakening and recovery of the area.

The restrictions exerted by the grafts, for the three cases of the different materials, are considerably lower than those generated by the original ACL, for all the variables evaluated and throughout the entire range. This indicates that the choice of graft diameter was not adequate, since a larger diameter would have caused the rigidity of the structure to increase, and consequently, for the same deformation, the forces exerted by the new graft would have been greater.

Regarding the ACLr with different femoral insertions, the results obtained when comparing the same graft for different femoral insertions show a considerable effect on the KJ forces. This causes great uncertainty and reveals that locating the femoral insertion of the graft is a challenging task. For all the variables studied, the graft located in the center of the original insertion of the ACL is the one that better fulfills the function of the natural ligament, obviating the previously expressed effect of the lack of cross-sectional area of the grafts. In addition, the anterior reconstruction model also shows the greatest difficulty to create a graft avoiding the PCL, causing high curvature radii and susceptible zones for stress concentration.

Comparing the loads of the three models (out of origin inserted) on the femur, a high variability is spotted. For instance, proximal reconstruction (pPTr) did not show very different results, in terms of forces, compared to origin reconstruction. However, in the graphs corresponding to the torques, a poor performance in the restriction of some movements is appreciated. This is clearly related to the direction in which the graft was oriented and not so much to the force it exerts. In the same way, significant changes result from the other two insertions, showing that the femoral insertion of the graft is one of the variables that requires more precision.

Authorship statement

The authors hereby confirm that they are the sole liable persons responsible for the authorship of this work and that all material that has been herein included as part of the present paper is either the property (and authorship) of the authors, or has the permission of the owners to be included here.

Acknowledgements The authors would like to thank to the Comisión Académica de Posgrado of the Universidad de la República of Uruguay, for the received support.

Funding The research leading to these results received funding from the Comisión Académica de Posgrado of the Universidad de la República of Uruguay.

Data availability Data presented in this paper are available for download in <https://rb.gy/dksxtc>

Code availability Not applicable.

Declarations

Ethics approval Approval of the Ethics Committee of the Universidad de la República was obtained for this study. Ethics committee clearance was applied for with number 151100–003630-17.

Consent to participate Informed consent was obtained from all individual participants included in the study.

Consent for publication Patients signed informed consent regarding publishing their data and photographs.

Conflicts of interest The authors have no conflicts of interest to declare that are relevant to the content of this article.

References

- Ali AA, Shalhoub SS, Cyr AJ, Fitzpatrick CK, Maletsky LP, Rulkoetter PJ, Shelburne KB. Validation of predicted patellofemoral mechanics in a finite element model of the healthy and cruciate-deficient knee. *J Biomech.* 2016;49(2):302–9.
- Andersen MS, Benoit DL, Damsgaard M, Ramsey DK, Rasmussen J. Do kinematic models reduce the effects of soft tissue artifacts in skin marker-based motion analysis? an in vivo study of knee kinematics. *J Biomech.* 2010;43(2):268–73.
- Andriacchi TP, Mikosz RP, Hampton SJ, Galante JO. Model studies of the stiffness characteristics of the human knee joint. *J Biomech.* 1983;16(1):23–9.
- Bae TS, Cho BC. Biomechanical effect of tunnel positions and pre-tension forces on implanted graft stress and strain during outside-in ACL reconstruction surgery: a simulation study. *Int J Precis Eng Manuf.* 2020;21(3):519–24.
- Barié A, Ehmann Y, Jaber A, Huber J, Streich NA. Revision ACL reconstruction using quadriceps or hamstring autografts leads to similar results after 4 years: good objective stability but low rate of return to pre-injury sport level. *Knee Surg Sports Traumatol Arthrosc.* 2019;27(11):3527–35.
- Bedi A, Musahl V, Steuber V, Kendoff D, Choi D, Allen AA, Pearle AD, Altchek DW. Transtibial versus anteromedial portal reaming in anterior cruciate ligament reconstruction: an anatomic and biomechanical evaluation of surgical technique. *Arthrosc: J Arthrosc Relat Surg.* 2011;27(3):380–90.
- Bistolfi A, Capella M, Guidotti C, Sabatini L, Artiaco S, Massè A, Ferracini R. Functional results of allograft vs. autograft tendons in anterior cruciate ligament (ACL) reconstruction at 10-year follow-up. *Eur J Orthop Surg Traumatol.* 2021;31(4), 729–735.
- Blankevoort L, Kuiper JH, Huiskes R, Grootenboer HJ. Articular contact in a three-dimensional model of the knee. *J Biomech.* 1991;24(11):1019–31.
- Bonin M, Amendola A, Bellemans J, MacDonald S, Menetrey J. The knee joint: Surgical techniques and strategies. 2012; <https://doi.org/10.1007/978-2-287-99353-4>.
- Butler DL, Guan Y, Kay MD, Cummings JF, Feder SM, Levy MS. Location-dependent variations in the material properties of the anterior cruciate ligament. *J Biomech.* 1992;25(5):511–8.
- Charlton I, Tate P, Smyth P, Roren L. Repeatability of an optimised lower body model. *Gait Posture.* 2004;20(2):213–21.
- Chen W, Li H, Chen Y, Jiang F, Wu Y, Chen S. Bone-Patellar Tendon–Bone Autografts Versus Hamstring Autografts Using the Same Suspensory Fixations in ACL Reconstruction: A Systematic Review and Meta-analysis. *Orthop J Sports Med.* 2019;7(11):2325967119885314.
- Chhabra A, Elliott CC, Miller MD. Normal anatomy and biomechanics of the knee. *Sports Med Arthrosc Rev.* 2001;9(3):166–77.
- Chiari L, Della Croce U, Leardini A, Cappozzo A. Human movement analysis using stereophotogrammetry: Part 2: Instrumental errors. *Gait Posture.* 2005;21(2):197–211.
- Cooper RJ, Wilcox RK, Jones AC. Finite element models of the tibiofemoral joint: A review of validation approaches and modelling challenges. *Med Eng Phys.* 2019;74:1–12.
- Crowninshield R, Pope MH, Johnson RJ. An analytical model of the knee. *J Biomech.* 1976;9(6):397–405.
- Dienst M, Burks RT, Greis PE. Anatomy and biomechanics of the anterior cruciate ligament. *Orthop Clin North Am.* 2002;33(4):605–20.
- Domenech RG, Moreno MC, Fernandez VM, Capel A. Anatomía y biomecánica de la articulación de la rodilla. Murcia: Servicio de Radiología, Facultad de Medicina Universidad de Murcia; 2003.
- Erdemir A. Open Knee: A Pathway to Community Driven Modeling and Simulation in Joint Biomechanics. *J Med Device.* 2013;7(4):0409101–409101. <https://doi.org/10.1115/1.4025767>
- Essinger JR, Leyvraz PF, Heegard JH, Robertson DD. A mathematical model for the evaluation of the behaviour during flexion of condylar-type knee prostheses. *J Biomech.* 1989;22(11–12):1229–41.
- Fernandes DJC. Finite element analysis of the ACL-deficient knee. Lisbon: University of Lisbon; 2014.

- Fregly BJ, Besier TF, Lloyd DG, Delp SL, Banks SA, Pandy MG, D'lima DD. Grand challenge competition to predict in vivo knee loads. *J Orthop Res*. 2012;30(4):503–13.
- Geuzaine C, Remacle J-F. Gmsh: A 3-d finite element mesh generator with built-in pre-and post-processing facilities. *Int J Numer Meth Eng*. 2009;79(11):1309–31.
- Girgis FG, Marshall JL, Monajem A. The cruciate ligaments of the knee joint. anatomical, functional and experimental analysis. *Clin Orthop Relat Res*. 1975;106:216–31.
- Halonen KS, Mononen ME, Jurvelin JS, Töyräs J, Salo J, Korhonen RK. Deformation of articular cartilage during static loading of a knee joint—experimental and finite element analysis. *J Biomech*. 2014;47(10):2467–74.
- Góngora García L, Rosales García C, González Fuentes I, Pujals Victoria N. Articulación de la rodilla y su mecánica articular. *Medisan*. 2003;7(2):100–09.
- Guo N, Wang T, Wei M, Hu L, Liu H, Wang Y, Yu G. An ACL reconstruction robotic positioning system based on anatomical characteristics. *Int J Adv Rob Syst*. 2020;17(1):1729881419886160.
- Halonen KS, Mononen ME, Töyräs J, Kröger H, Joukainen A, Korhonen RK. Optimal graft stiffness and pre-strain restore normal joint motion and cartilage responses in ACL reconstructed knee. *J Biomech*. 2016;49:2566–76. <https://doi.org/10.1016/j.jbiomech.2016.05.002>.
- Jakob RP, Staübli H. *The Knee and the cruciate ligaments: anatomy, biomechanics, clinical aspects, reconstruction, complications, rehabilitation*. Springer; 1992.
- Kadaba MP, Ramakrishnan H, Wootten M. Measurement of lower extremity kinematics during level walking. *J Orthop Res*. 1990;8(3):383–92.
- Kazemi M, Dabiri Y, Li LP. Recent advances in computational mechanics of the human knee joint. *Comput Math Methods Med*. 2013;718423. <https://doi.org/10.1155/2013/718423>.
- Kim S, Bosque J, Meehan JP, Jamali A, Marder R. Increase in outpatient knee arthroscopy in the United States: a comparison of national surveys of ambulatory surgery, 1996 and 2006. *J Bone Joint Surg*. 2011;93(11):994–1000.
- Kim SH, Kim SJ, Choi CH, Kim D, Jung M. Optimal condition to create femoral tunnel considering combined influence of knee flexion and transverse drill angle in anatomical single-bundle ACL reconstruction using medial portal technique: 3d simulation study. *Biomed Res Int* 2018;2643247. <https://doi.org/10.1155/2018/2643247>.
- Leardini A, Chiari L, DellaCroce U, Cappozzo A. Human movement analysis using stereophotogrammetry: Part 3. Soft tissue artifact assessment and compensation. *Gait Posture*. 2005;21(2):212–25.
- Li G, Gil J, Kanamori A, Woo SL. A validated three-dimensional computational model of a human knee joint. *J Biomech Eng*. 1999;121(6):657–62. <https://doi.org/10.1115/1.2800871>.
- Łuczkiwicz P, Daszkiewicz K, Witkowski W, Chrościelewski J, Zarzycki W. Influence of meniscus shape in the cross sectional plane on the knee contact mechanics. *J Biomech*. 2015;48(8):1356–63.
- Maas SA, Ellis BJ, Ateshian GA, Weiss JA. FEBio: finite elements for biomechanics. *J Biomech Eng*. 2012;134(1):011005. <https://doi.org/10.1115/1.4005694>.
- Mallett KF, Arruda EM. Digital image correlation-aided mechanical characterization of the anteromedial and posterolateral bundles of the anterior cruciate ligament. *Acta Biomater*. 2017;56:44–57.
- Marieswaran M, Jain I, Garg B, Sharma V, Kalyanasundaram D. A Review on Biomechanics of Anterior Cruciate Ligament and Materials for Reconstruction. *Appl Bionics Biomech*. 2018;4657824. <https://doi.org/10.1155/2018/4657824>.
- Markolf KL, Burchfield DM, Shapiro MM, Shepard MF, Finerman GA, Slauterbeck JL. Combined knee loading states that generate high anterior cruciate ligament forces. *J Orthop Res*. 1995;13(6):930–5.
- Marra M. Personalized musculoskeletal modeling of the knee joint. PhD thesis, Universidad Radboud Nijmegen. Radboud Repository. 2019. <https://repository.ubn.ru.nl/bitstream/handle/2066/201897/201897.pdf>.
- McLean SG, Mallett KF, Arruda EM. Deconstructing the anterior cruciate ligament: what we know and do not know about function, material properties, and injury mechanics. *J Biomech Eng*. 2015;137(2):020906. <https://doi.org/10.1115/1.4029278>.
- Meng Q, Jin Z, Wilcox R, Fisher J. Computational investigation of the time-dependent contact behaviour of the human tibiofemoral joint under body weight. *Proc Inst Mech Eng [h]*. 2014;228(11):1193–207.
- Meng Q, An S, Damion RA, Jin Z, Wilcox R, Fisher J, Jones A. The effect of collagen fibril orientation on the biphasic mechanics of articular cartilage. *J Mech Behav Biomed Mater*. 2017;65:439–53.
- Miller SL, Gladstone JN. Graft selection in anterior cruciate ligament reconstruction. *Orthopedic Clinics*. 2002;33(4):675–83.
- Mononen ME, Tanska P, Isaksson H, Korhonen RK. A novel method to simulate the progression of collagen degeneration of cartilage in the knee: data from the osteoarthritis initiative. *Sci Rep*. 2016;6(1):1–14.
- Mootanah R, Imhauser CW, Reisse F, Carpanen D, Walker RW, Koff MF, Hillstrom HJ. Development and validation of a computational model of the knee joint for the evaluation of surgical treatments for osteoarthritis. *Comput Methods Biomech Biomed Engin*. 2014;17(13):1502–17.
- Naghbi Beidokhti H. Personalized Finite element models of the knee joint: a platform for optimal orthopedic surgery pre-planning. PhD thesis, Universidad Radboud Nijmegen. Radboud Repository. 2018. <https://repository.ubn.ru.nl/bitstream/handle/2066/196839/196839.pdf>.
- Noyes FR, DeLucas JL, Torvik PJ. Biomechanics of Anterior Cruciate Ligament Failure: An Analysis of Strain-Rate Sensitivity and Mechanisms of Failure in Primates. *J Bone Joint Surg Am*. 1974;56:236–53.
- Panesso MC, Trillos MC, Guzmán IT. *Biomecánica clínica de la rodilla (Documento de investigación Núm. 39)*. Universidad del Rosario-Facultad de Rehabilitación y Desarrollo Humano. 2018. <https://core.ac.uk/download/pdf/86435349.pdf>.
- Pena E, Martinez M, Calvo B, Palanca D, Doblare M. A finite element simulation of the effect of graft stiffness and graft tensioning in acl reconstruction. *Clin Biomech*. 2005;20(6):636–44.
- Pena E, Calvo B, Martinez M, Doblare M. A three-dimensional finite element analysis of the combined behavior of ligaments and menisci in the healthy human knee joint. *J Biomech*. 2006;39(9):1686–701.
- Rachmat HH. Towards a subject-specific knee model to optimize ACL reconstruction. PhD thesis, University of Groningen. UMG research database. 2015. https://pure.rug.nl/ws/portafiles/porta/16426994/Complete_dissertation.pdf.
- Räsänen LP, Tanska P, Zbyň Š, van Donkelaar CC, Trattinig S, Nieminen MT, Korhonen RK. The effect of fixed charge density and cartilage swelling on mechanics of knee joint cartilage during simulated gait. *J Biomech*. 2017;61:34–44.
- Rothrauff BB, Jorge A, de Sa D, Kay J, Fu FH, Musahl V. Anatomic ACL reconstruction reduces risk of post-traumatic osteoarthritis: a systematic review with minimum 10-year follow-up. *Knee Surg Sports Traumatol Arthrosc*. 2020;28(4):1072–84.
- Santos D. Estudio de los centros de rotación instantáneos de la rodilla en pacientes con plastia de ligamento cruzado anterior. MSc thesis, Universidad de la República (Uruguay). Facultad de Medicina. Colibrí. 2014. <https://www.colibri.udelar.edu.uy/jspui/handle/20.500.12008/4308>.

- Sibole S, Bennetts C, Borotikar B, Maas S, van den Bogert AJ, Weiss JA, Erdemir A. Open knee: a 3D finite element representation of the knee joint, 34th Annual Meeting of the American Society of Biomechanics, August 18–21, 2010, Providence, RI.
- Shelburne KB, Pandy MG, Anderson FC, Torry MR. Pattern of anterior cruciate ligament force in normal walking. *J Biomech.* 2004;37(6):797–805.
- Shirazi R, Shirazi-Adl A. Computational biomechanics of articular cartilage of human knee joint: effect of osteochondral defects. *J Biomech.* 2009;42(15):2458–65.
- Shu L, Yamamoto K, Yao J, Saraswat P, Liu Y, Mitsuishi M, Sugita N. A subject-specific finite element musculoskeletal framework for mechanics analysis of a total knee replacement. *J Biomech.* 2018;77:146–54.
- Siebold R, Dejour D, Zaffagnini S. Anterior Cruciate Ligament Reconstruction: A Practical Surgical Guide. 2014. <https://doi.org/10.1007/978-3-642-45349-6>.
- Stief F, Böhm H, Michel K, Schwirtz A, Döderlein L. Reliability and accuracy in three-dimensional gait analysis: a comparison of two lower body protocols. *J Appl Biomech.* 2013;29(1):105–11.
- Suggs J, Wang C, Li G. The effect of graft stiffness on knee joint biomechanics after acl reconstruction: a 3d computational simulation. *Clin Biomech.* 2003;18(1):35–43.
- Tashman S, Zandiyeh P, Irrgang JJ, Musahl V, West RV, Shah N, Fu FH. Anatomic single- and double-bundle ACL reconstruction both restore dynamic knee function: a randomized clinical trial-part II: knee kinematics. *Knee Surg Sports Traumatol Arthrosc: Official Journal of the ESSKA.* 2021;29(8):2676–83. <https://doi.org/10.1007/s00167-021-06479-x>.
- Todor A, Nistor DV, Caterev S. Clinical outcomes after ACL reconstruction with free quadriceps tendon autograft versus hamstring tendons autograft. A retrospective study with a minimal follow-up two years. *Acta Orthop Traumatol Turc.* 2019;53(3):180–83. <https://doi.org/10.1016/j.aott.2019.03.004>.
- Trad Z, Barkaoui A, Chafra M, Tavares JMR. FEM analysis of the human knee joint: a review. Springer; 2018.
- VICON Motion Systems. Plug-in gait reference guide, 2017. <https://docs.vicon.com/download/attachments/42696722/Plug-in%20Gait%20Reference%20Guide.pdf?version=1&modificationDate=1502364735000&api=v2>.
- Weiss JA. A constitutive model and finite element representation for transversely isotropic soft tissues. PhD thesis, The University of Utah. Musculoskeletal Research Laboratories. 1994. https://mrl.sci.utah.edu/papers/jaw_diss.pdf.
- Weiss JA, Maker BN, Govindjee S. Finite element implementation of incompressible, transversely isotropic hyperelasticity. *Comput Methods Appl Mech Eng.* 1996;135(1–2):107–28.
- Weiss JA, Gardiner JC, Bonifasi-Lista C. Ligament material behavior is nonlinear, viscoelastic and rate-independent under shear loading. *J Biomech.* 2002;35(7):943–50.
- Wismans JAC, Veldpaus F, Janssen J, Huson A, Struben P. A three-dimensional mathematical model of the knee-joint. *J Biomech.* 1980;13(8):677–85.
- Xiao Y, Ling M, Liang Z, Ding J, Zhan S, Hu H, Chen B. Dual fluoroscopic imaging and CT-based finite element modelling to estimate forces and stresses of grafts in anatomical single-bundle ACL reconstruction with different femoral tunnels. *Int J Comput Assist Radiol Surg.* 2021;16(3):495–504.

Publisher's note Springer Nature remains neutral with regard to jurisdictional claims in published maps and institutional affiliations.